2022 19th International Conference on Ubiquitous Robots (UR)
July 4-6, 2022. Ramada Plaza Jeju, Jeju, Korea

2022 19th International Conference on Ubiquitous Robots (UR) | 978-1-6654-8253-0/22/$31.00 ©2022 IEEE | DOI: 10.1109/UR55393.2022.9826288

A Sensor Fusion Strategy for Indoor Target Three-dimensional Localization based on Ultra-Wideband and Barometric Altimeter Measurements

Le Bao, Kai Li, Wenqi Li, Kyoosik Shin, and Wansoo Kim*, *Member, IEEE*

***Abstract*—Obtaining relative spatial localization information of target objects is crucial in scenarios such as robotics operations and augmented reality. In this paper, a strategy based on data fusion of ultra-wideband (UWB) sensors and barometric pressure (BMP) sensors are proposed to identify the three-dimensional (3D) localization information of indoor targets. The height estimation of the target is calculated from the difference in barometric pressure measured by two high-precision BMP sensors. The measured height values with the distance values measured by the UWB sensors are used to target localization based on a geometric model. Finally, the localization is dynamically optimized by triangle center-of-mass method and Kalman filtering. Based on the designed indoor 3D localization system, the target node's location measurement information in the stationary state, and the trajectory information obtained from localization in the motion state are obtained and compared with the actual location. The experimental results show that the sensor fusion system can achieve real-time localization and trajectory recording, which is convenient for scenarios such as robot operation.**

I. INTRODUCTION

Localization technology is an important part for robots to perceive the environment, obtaining precision location information can help robots achieve more accurate unmanned operation or human-robot interaction [1-3].

Wireless sensors commonly used for ranging and localization include Wi-Fi, Bluetooth, ultra-wideband (UWB), radio frequency identification (RFID), millimeter-wave radar, ultrasonic radar, and so on, which measure distance by received signal strength Indication (RSS) or communication time [4-9]. UWB sensor has a wider measurement range compared to Bluetooth and RFID, and stronger anti-interference performance compared to Wi-Fi [10]. Because of the advantages of UWB's anti-multipath effect, high penetration, low power consumption and high range accuracy [11-12], UWB technology is widely used in smart factories for localization and management of equipment or personnel, smart training in stadiums and other places where precise localization is required [13-15]. UWB sensors measure distance by calculating the time spent in communication of transmitting and receiving very short pulse signals [16]. The UWB localization method generally arranges three or more base stations in the environment, and the measurement and calculation of distance information between the target and each base station to achieve accurate localization of the target [17-18].

Compared to single sensor ranging, multi-sensor data fusion is attracting increasing attention because it can combine the advantages of different sensors to obtain more accurate and stable information [19]. Yang et al. proposed a non-line of sight (NLOS) error compensation method for UWB indoor localization by combining acceleration data from an inertial measurement unit (IMU) to improve the accuracy of the localization system [20]. Similarly [21] has been studied two-dimensional (2D) planar space localization, which leads to errors when applied to actual three-dimensional (3D) spatial scenes [22].

In this paper, a multi-sensor fusion strategy based on ultra-UWB sensors and high-precision barometric pressure (BMP) sensors for indoor 3D spatial localization method is proposed. To improve the accuracy of UWB localization in indoor 3D spatial, we use dual BMP Sensors to estimate the altitude of the target and fuse it in the UWB 3D localization model. First, we designed the structure of marking the base coordinates and fixed three UWB base stations in this frame that determines the relative locations, which is more portable and convenient compared to the decentralized base stations setup method. Moreover, the distance data of the measured target location and the three UWB base stations were rectified and filtered to improve the accuracy of the raw UWB data. For the barometric altimeter measurement, the data of the barometric altimeter at the target is transmitted to the base coordinate localization system through the WiFi wireless communication function [23] of the ESP8266 chip, and we tested and found that the data drift changes of the barometric pressure values from two BMP sensors with the same model in the same indoor space tend to be consistent, and the altitude values of the target barometer are estimated from the difference between the barometers data.

Based on the geometric model, the BMP sensor is fused with the UWB sensor to derive three sets of coordinate estimates of the target locations. The best estimates of the target node locations are obtained by triangle center-of-mass algorithm and Kalman filtering, and the trajectory of localization is made more accurate and smooth.

This work was supported by the National Research Foundation of Korea(NRF) grant funded by the Korea government(MSIT) (No. 2022R1C1C1008306). L. Bao is grateful for financial support of the China Scholarship Council (No. 202108260014).

*Wansoo Kim is with the Department of Robot Engineering, Hanyang University, Ansan, Gyeonggi-do 15588, Republic of Korea (corresponding author to provide phone: 031-400-4062; fax: 031-406-6398; e-mail: wansookim@hanyang.ac.kr).

Le Bao, Kai Li, and Wenqi Li are with the Department of Mechatronics Engineering, Hanyang University, Ansan, Gyeonggi-do 15588, Republic of Korea (e-mail: {baole, likai5289, liwenqi}@hanyang.ac.kr).

Kyoosik Shin is with the Department of Robot Engineering, Hanyang University, Ansan, Gyeonggi-do 15588, Republic of Korea (e-mail: norwalk87@hanyang.ac.kr).

Our main contributions are:

- The distance data measured by the UWB sensor device is filtered and corrected, and the sensor distance measurement accuracy is obtained 3 cm.
- Comparing two barometers in an indoor environment with the same trend of data drift, the altitude estimated by the barometer difference is more accurate compared to the data measured from a single barometric value.
- Verified the possibility of a sensor fusion strategy based on UWB sensors and BMP sensors for 3D localization, which provides a new solution for target localization in robotics operations, augmented reality (AR), and other fields.

The concrete structure of this paper is as follows: The second part describes the hardware of multi-sensor localization system. The third part introduces the target localization based on data fusion strategy. The fourth part verifies the effectiveness of the algorithm through specific experiments. The fifth part summarizes the results of this study, expounds the advantages and disadvantages of the system, and presents future work.

II. Hardware System

This study designs an indoor 3D localization system combining UWB range sensor and BMP altitude sensor. The system consists of a UWB ranging module group, two high-precision barometric altitude sensors with the same type, two ESP8266 modules for wireless data transmission, and power supply modules, and the system is divided into two parts: the base station frame (Fig. 1(a)) and the target frame (Fig. 1(b)). The coordinate location of the localization measurement is relative to the base coordinate origin in the base station frame.

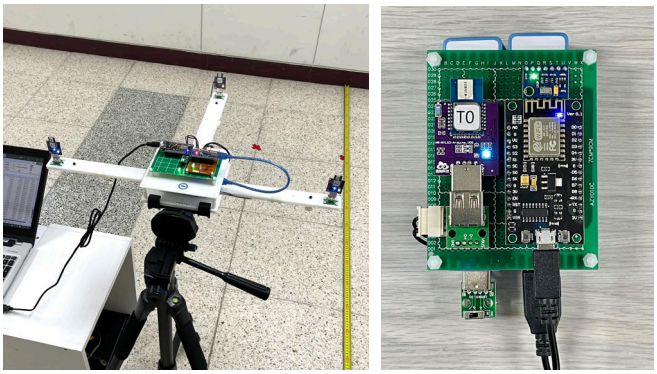

(a) The base station frame. (b) The target frame.

Figure 1. Indoor 3D localization system hardware.

A. UWB Sensor Distance Measurement

The UWB module used in this study uses a DW1000 chip manufactured by DecaWAVE with centimeter-level ranging accuracy. The processor of the module reads the raw data from the chip, converts the data into distance values between the UWB target node and each UWB base station node using the time difference of arrival (TDOA) algorithm, and sends the ranging data through serial communication.

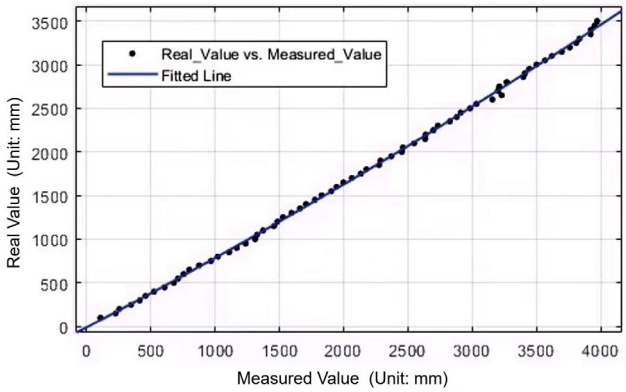

Figure 2. Data correction of UWB ranging module.

There is an error between the measured value of this UWB sensor and the actual value, and the error value tends to increase as the real distance value increases. Our correction work records the average of 250 filtered range measurements between the UWB target node and the UWB base station node every 0.05 m within a range of 3.5 m, and compares the recorded measurement data from the UWB module output with the actual distance value, the three fitting equations for correcting the measured output value of this UWB module were obtained separately by the data fitting function of MATLAB's Curve Fitting Toolbox. As shown in Fig. 2, the fitted equation can be defined as:

$$D_{fit} = 2.4\times10^{-5}\times D_{raw}^{2} + 0.7725\times D_{raw} - 12.38 \ , \qquad (1)$$

where D_{raw} is the raw data output from the UWB module and D_{fit} is the fitted corrected data.

The error variation problem was solved by the correction process. After the distance measurement data of the UWB sensor was filtered and corrected, the noise fluctuation of the static measurement value was reduced from a large change of about 10 cm to about 3 cm, and the stability and accuracy of the UWB module distance measurement was improved.

B. Dual BMP Sensors Height Measurement

The BMP sensor used is the MS5611 high-resolution sensor introduced by MEAS company. The measured barometric pressure and temperature data are used to obtain the altitude value of the measurement location [24] by using:

$$H_{baro} = \left(1-\left(\frac{P_{baro}}{P_0}\right)^{0.19}\right)\times\left(\frac{T+273.15}{0.0065}\right) \ , \qquad (2)$$

where H_{baro} is the altitude value measured in meters, P_{baro} is the barometric pressure value measured in Pa, and P_0 is the reference value of barometric pressure at sea level and it is equal to 101325 Pa in normal conditions, T is the temperature in °C.

Airflow, temperature, and other factors can affect the performance of the BMP sensor, for this reason, the measured values of two MS5611 BMP sensors in the same indoor environment were tested. As shown in Fig. 3, the raw barometer data are successively processed by weighted average filtering and Kalman filtering to remove the noisy data.

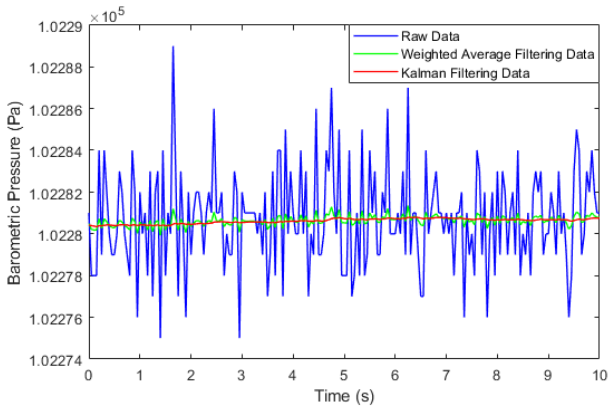

Figure 3. Filtering of barometric pressure measurement data.

The target BMP sensor is placed at a straight line distance of 2 meters from the base station BMP sensor with a height difference of 0.5 m, and their barometric data comparison and height estimation are shown in Fig. 4. Within one hour of the test, the two BMP sensors drifted by 5.56 m and 5.21 m, respectively, and it can be observed that the estimated height value of the BMP sensor decreases with the increase of the barometric pressure measurement.

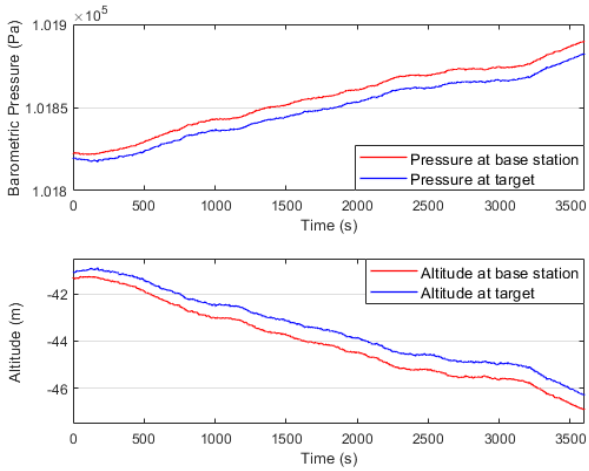

Figure 4. Measurement data of dual BMP sensors in one hour.

While the barometric pressure values measured by sensors at the same time and the estimated altitude values have the same overall trend, after the initial barometric pressure values of the target BMP sensor and the base station BMP sensor are calibrated, the data drift of the estimated altitude values occurred by the difference calculation is only 0.46 m within one hour, and the data drift in a short time is mostly offset. The estimated altitude is more accurate compared to the single sensor, and the frequency of barometer correction can be reduced over a long period of time.

The barometric pressure data at the target location is sent to the main processor at the base coordinates through the WiFi wireless communication function of the ESP8266 chip. The height value (H_{target}) estimated by the dual BMP sensors is:

$$H_{target} = \left(\left(\frac{P_{base}}{P_0} \right)^{0.19} - \left(\frac{P_{target}}{P_0} \right)^{0.19} \right) \times K_{temp} \ , \qquad (3)$$

where P_{base} is the barometric pressure value measured at the base station location, P_{target} is the barometric pressure value at the target location, the unit measurement of the barometer is Pa, and P_0 is the reference value of the barometric pressure at sea level, and the temperature parameter value K_{temp} is set to 44330 due to the small effect of the temperature change on the height estimation in the indoor environment.

Before estimating the altitude, the calibration of the initial barometric pressure value of the target location BMP sensor is achieved by keeping the target location BMP sensor at the same height as the BMP sensor at the base coordinate origin and close to any of the UWB base station nodes.

C. Localization System Structure

The structure of the system is shown in Fig. 5, the base station framework contains three UWB base station nodes (UWB_B1, UWB_B2, UWB_B3), the BMP base station node (BMP_B1) and the controller module as a server. The target frame contains a UWB target node (UWB_T1), BMP target node (BMP_T1) and the main controller module as a client. The power supply of the system is provided by rechargeable batteries.

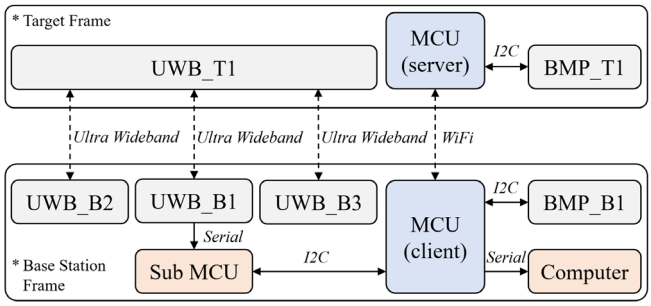

Figure 5. System structure diagram.

UWB_B1 is fixed at the location 0.31 m in the negative direction of x-axis, UWB_B2 and UWB_B3 are set respectively at the location 0.26 m in the positive and negative direction of y-axis in the base coordinate system. The communication between UWB sensors is based on ultra-wideband, and the measured three distance values are sent to the sub microcontroller (Sub MCU) uniformly by the serial port (UART) of UWB_B1, and sent via I2C communication when the main MCU requests data from the sub MCU.

The BMP base station node B1 is set at the origin of the coordinate axis, and the barometric pressure value measured by the BMP sensor is transmitted to the controller via I2C communication. The server microcontroller (MCU(server)) generates the server data from the collected data of the BMP target node T1, and reads it by the client main microcontroller (MCU(client)) via WiFi communication.

Eventually, the target 3D location information estimated by the main controller based on the fusion algorithm is sent to the computer recording the data through the serial port. The hardware parameters of the sensors used in the system are shown in Table 1 and the parameters of the controller used are shown in Table 2.

TABLE I. SENSOR HARDWARE PARAMETERS

Sensor Types	Ultra-Wideband Sensor	Barometric Pressure Sensor
Model	DW1000	MS5611
Names in the System	UWB_(B1, B2, B2, T1)	BMP_(B1, T1)
Working Voltage	5 [V]	3.3 [V]
Communication Mode	Ultra-wideband, UART	I2C
Measuring Speed	4 [Hz]	20 [Hz]

TABLE II. MICROCONTROLLER HARDWARE PARAMETERS

Microcontroller Model	NodeMCU	Arduino Nano
Processing Chip	ESP8266	ATmega328P
Names in the System	MCU(client), MCU(server)	Sub MCU
Working Voltage	5 [V]	5 [V]
Communication Mode	UART, I2C, WiFi	UART, I2C
Serial Communication Speed	115200 [Hz]	115200 [Hz]

III. SENSOR FUSION LOCALIZATION STRATEGY

A. 3D Localization based on Sensor Fusion

Since UWB sensors cannot directly estimate the height variation, the 3D localization algorithm based on UWB sensors requires at least four UWB base stations and uses more UWB sensor ranging base stations to increase the localization accuracy [25]. As for the 2D planar localization algorithm for UWB sensors, ignoring the variation of the actual target location in the vertical direction will reduce the accuracy of planar localization. In this study, the designed method of measuring height with dual BMP sensors has good indoor height estimation performance, so we propose to use dual BMP sensors to improve the accuracy of 3D localization using only three UWB base stations.

In the geometric model of the 3D localization system shown in Fig. 6, three UWB base station nodes UWB_B2, UWB_B3, and UWB_B1 are located respectively at three points *A(0, -OA, 0)*, *B(0, OB, 0)*, and *C(-OC, 0, 0)*, and the distance lengths *AP*, *BP*, and *CP* between them and the UWB target node P are measured by the UWB sensors. The distance length PQ between the target node location P and the coordinate axis x-y plane is the absolute value of the height value H_{target} estimated by the dual barometric sensors.

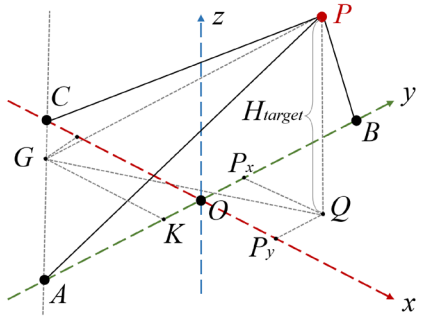

Figure 6. Geometric model of 3D localization system.

In practical measurements, the estimated target node P often lies in the range of a spatial region due to the error of UWB sensor ranging, and the triangle center-of-mass method can be used to estimate to a more accurate localization value. Under the model of Fig. 7, the estimated target location can be located at any point on the circular intersection line of the sphere formed by the distance measured by any two UWB base stations. The gray part of the figure shows a plane formed by the height values measured by the BMP sensors, which can determine the target location at two specific location points on this circular intersection line. Considering that in some cases the error of the UWB sensor range may cause the two spheres not to intersect, the location of the target point is set to the middle of the non-intersecting outer sphere and inner sphere in the calculation of this model.

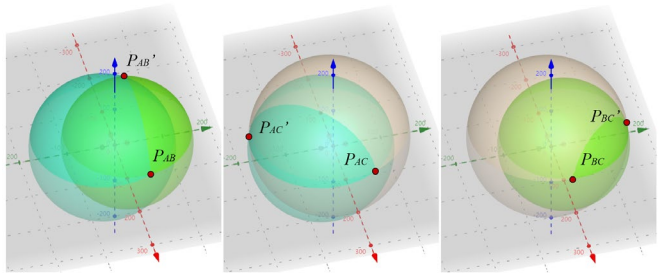

(a) Base station A and B. (b) Base station A and C. (c) Base station B and C.

Figure 7. Target point locations estimated by any two UWB base stations with BMP sensors.

In the geometric relationship between UWB base station *A* and *C* as in Fig. 6, the point P_{AC} perpendicular *x-y* plane at point *Q*, $P_{AC}G$ perpendicular *AC* intersects at point *G*, *GK* perpendicular y-axis intersects at point *K*. The size of the area of triangle ACP_{AC} can be obtained from Heron's formula (4) and calculated to the length of the high GP_{AC}, and the length of *AG* is found in triangle AGP_{AC} using the Pythagorean theorem.

$$f = 0.5 \times (AC + AP + CP) \ , \quad S_{\Delta ACP_{AC}} = \sqrt{f \times (f - AC) \times (f - AP_{AC}) \times (f - CP_{AC})} \ . \tag{4}$$

By comparing the lengths of AP_{AC} and CP_{AC}, the location of point *G* on the *AC* line relative to points *A* and *C* is analyzed. In the case *G* in this figure is located between *AC*, then the coordinates of point *G* are obtained based on the coordinates of point A. In the triangle $GP_{AC}Q$ use the Pythagorean theorem to find the length of *GQ* and obtain the coordinates of point *Q* through the geometric relationship, that is, the coordinates of the P_{AC} point on the x-axis and y-axis. In addition, find the other intersection point P_{AC}' on the other side of the straight line *AC* as in Fig. 7(b). Similarly, the coordinates of the intersection location P_{AB}, P_{AB}', P_{BC} and P_{BC}' of UWB base station *A* and *B* or UWB base station *B* and *C* can be obtained.

The main controller calculates three sets of six intersection locations obtained from the two UWB base station ranges and the altitude values measured respectively by the BMP sensors, and obtains the coordinates of the three closest points in the three sets of data to obtain P_{AB}, P_{AC}, P_{BC}, and thus the estimated best target location coordinates $P(P_x, P_y, P_z)$ expressed as:

$$\begin{cases} P_x = \frac{1}{3} \times \left(P_{AB\_x} + P_{AC\_x} + P_{BC\_x} \right) \\ P_y = \frac{1}{3} \times \left(P_{AB\_y} + P_{AC\_y} + P_{BC\_y} \right) \\ P_z = H_{target} \end{cases} . \tag{5}$$

B. Kalman Filter based Location Estimation Optimization

However, the sensor fusion localization system is affected by the data fluctuation of sensors and the environment, the trajectory composed of target location points calculated by the geometric model will have errors with the actual value. In order to optimize the location estimation of the target node, the monitoring of the time variation quantity $\triangle t$ is added to the operation of the localization system, and the displacement s, velocity v, and acceleration a of the target node are calculated by combining the before-and-after location information, and another Kalman filter method is used to analyze the before-and-after motion information of the target node to predict and update the coordinates of the target location.

The prediction part of the Kalman filter calculates the a priori estimate (6) and the prediction error covariance (7), using the best estimate X_{t-1}^* at the previous moment *(t-1)* and the external control quantity U_t to obtain the a priori estimate X_t' at the current moment t, and using the updated system covariance P_{t-1} at the previous moment and the system process noise Q to obtain the a priori error covariance P_t' at the current moment.

$$X_t' = E \cdot X_{t-1}^* + F \cdot U_t \ , \tag{6}$$

$$P_t' = E \cdot P_{t-1} \cdot E^T + Q \ , \tag{7}$$

where

$$E = \begin{bmatrix} 1 & \Delta t & 0 & 0 & 0 & 0 \\ 0 & 1 & 0 & 0 & 0 & 0 \\ 0 & 0 & 1 & \Delta t & 0 & 0 \\ 0 & 0 & 0 & 1 & 0 & 0 \\ 0 & 0 & 0 & 0 & 1 & \Delta t \\ 0 & 0 & 0 & 0 & 0 & 1 \end{bmatrix}, \quad F = \begin{bmatrix} \Delta t^2/2 & 0 & 0 \\ \Delta t & 0 & 0 \\ 0 & \Delta t^2/2 & 0 \\ 0 & \Delta t & 0 \\ 0 & 0 & \Delta t^2/2 \\ 0 & 0 & \Delta t \end{bmatrix},$$

$$X_{t-1}^* = \begin{bmatrix} s_{x_{t-1}} & v_{x_{t-1}} & s_{y_{t-1}} & v_{y_{t-1}} & s_{z_{t-1}} & v_{z_{t-1}} \end{bmatrix}', \quad U_t = \begin{bmatrix} a_x \\ a_y \\ a_z \end{bmatrix},$$

and E is the state transfer matrix, F is the control matrix, and the system process noise Q is set to *diag(0.03, 0.03, 0.03, 0.03, 0.03, 0.03)*.

The update part of Kalman filter consists of Kalman gain, optimal estimate, and update system covariance. The displacement, velocity, and acceleration of the target node are taken as the system observations, and the system observation equation is established, and the Kalman gain Kg_t at time t, the optimal estimate X_t^*, and the update system covariance P_t at time t are calculated using the a priori estimate X_{t-1}' and the a priori error covariance P_t' of the prediction part and the system observation Z_t at this moment, which are calculated as (8-11):

$$Z_t = H \cdot X_t + V_t \ , \tag{8}$$

$$Kg_t = \frac{P_{t-1}' \cdot H^T}{H \cdot P_{t-1}' \cdot H^T + R} \ , \tag{9}$$

$$X_t^* = X_t' + Kg_t \cdot \left(Z_t - H \cdot X_t' \right) \ , \tag{10}$$

$$P_t = \left(I - Kg_t \cdot H \right) \cdot P_t' \ , \tag{11}$$

where H is the measurement system parameter, I is a unit matrix, and the observation covariance R is set to *diag(1, 1, 1, 1, 1, 1)*. Consequently, the coordinate values of the target node locations are optimized by Kalman filtering.

IV. Experiments and Analysis

In order to verify the performance of the proposed 3D localization system, localization experiments and data analysis were performed in the stationary and moving states of the target nodes.

A. Static Target Localization

The target node was placed at a stationary location in indoor space, and the actual coordinates of the target node with respect to the base station system were (1.80, 0.75, 0.45) m. 3671 sets of localization data were obtained through a long time test of 20 minutes. The comparison of the coordinate data identified by the localization system, the Kalman filter-optimized coordinate data, and the actual coordinate data is shown in Fig. 8, with the same scale range in the figure.

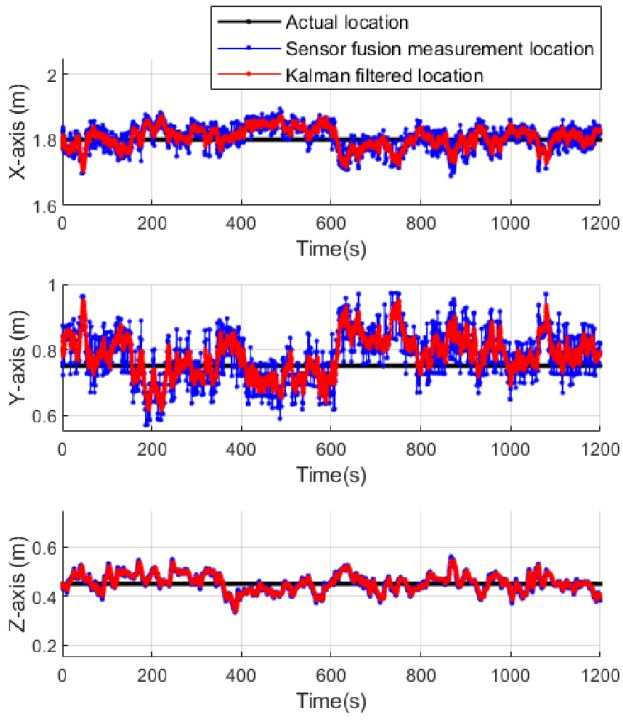

Figure 8. Static target localization results.

The target localization estimation on x-axes and y-axes was based on the estimation of altitude by the dual BMP sensors. The experimental result data were relatively stable on x-axes and z-axes, while the data on y-axes fluctuate in a slightly larger range. The analysis of experimental data for static target localization is shown in Table 3. The superiority of the designed dual BMP sensors for height measurement over a long period of time compared to the single BMP sensor can be observed again through the graphs and tables.

TABLE III. ANALYSIS OF THE STATIC TARGET LOCALIZATION RESULTS

Coordinates	Actual Value [m]	Average Value [m]	Maximum Error [m]	Standard Deviation
X-axis	1.800	1.805	0.116	3.519
Y-axis	0.750	0.781	0.212	7.213
Z-axis	0.450	0.454	0.121	3.626

When the error of the y-axis coordinates is maximum, the error distance from the actual coordinates is 0.1976 m. However, the maximum errors of x-axis, y-axis, and z-axis do not occur simultaneously, and the error distance between the coordinates expressed by the average value of the measurement and the coordinate of the actual location is 0.032 m. On the other hand, if the target node can be judged to be at stationary state, the accuracy of static target localization can be improved by calculating the average of its output coordinates.

B. Moving Target Localization Trajectory

To test the localization effect of the target localization system in 3D space, the moving reference path was set as the edges of two mutually perpendicular rectangles, which can detect the target movement in six directions in three dimensions. The target node moved along the set path. The experimental results of the moving target localization trajectory are shown in Fig. 9, where the black line is the actual moving reference path, the blue line is the location trajectory estimated by sensor fusion, and the red line is the final trajectory optimized by Kalman filtering, and the coordinates of the initial point of the location trajectory estimated by sensor fusion are (0.8631, -0.5803, - 0.3176) m, and the coordinates of the end point are (0.8754, -0.5826, -0.3208) m.

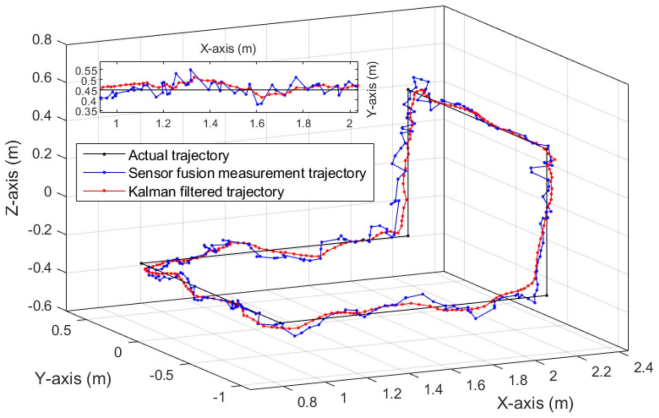

Figure 9. Moving target localization results.

The distance data measured using only three UWB sensors cannot determine the positive or negative of altitude, and part of the data cannot be calculated to the real number solution of the target altitude due to the accumulation of measurement errors. In this paper, the dual BMP sensors method was designed to analyze the height value of the target more reliably and estimated the coordinates of the target by the designed 3D localization strategy.

The result shows that the coordinate trajectory output by the localization system is in good alignment with the reference path as a whole, and the trajectory before the end of the trajectory is again close to and almost coincides with the trajectory after the starting location. The final trajectory optimized by Kalman filtering combining velocity and acceleration changes can reduce the influence of larger error points and smooth out the overall target node motion trajectory as can be seen more clearly in the local enlarged view of x-y plane. The experiment verifies the stability of the system in measuring vertical height and the accuracy of 3D spatial localization.

The corrected UWB sensors can measure targets within a radius of 3.5 meters, and more correction of UWB sensor measurements is needed for indoor localization in the face of longer ranges. Meanwhile, for dynamic target localization, the unstable airflow generated when the target suddenly moves or rotates can cause small changes in the barometric pressure measured by the target BMP sensor, which has a transient effect on the altitude estimation.

V. CONCLUSION

In this paper, we presented a sensor fusion strategy for indoor 3D localization of target node based on UWB ranging sensors and BMP height sensors. This provides a new measurement method for target localization. The base station node and the target node transmit the information acquired by the sensors through wireless communication. Two high-precision BMP sensors measure the relative location height, and two of the three UWB sensors obtain three sets of estimates of the target node location coordinates based on the geometric model, respectively, and use the triangle center-of-mass method to obtain the best estimate, and then use Kalman filtering to further optimize the 3D localization of the target node to achieve dynamic trajectory tracking of the target nodes.

Compared with [26] on improving the performance of height estimation by a single BMP sensor using UWB sensors, our study removes most of the BMP sensor measurement noise by filters, and estimated altitude from the differential barometric pressure values identified from the dual BMP sensors, and observes that the data drift of the height values estimated by the dual BMP sensors within one hour is only about one-twelfth of the data drift by a single BMP sensor. This greatly improves the observation of altitude values by the BMP sensors and provides a more accurate localization accuracy based on sensor fusion.

In addition, only three UWB sensor base stations are used in this study, which reduces the cost compared to the method of using at least four or more UWB base stations to improve 3D localization accuracy. The designed indoor 3D localization strategy can be applied to robot operation, scene understanding, and augmented reality.

Future research plans to analysis multipath effects by UWB signal intensity information, fuse IMU sensors to obtain more target localization reference information, and verify the location estimation performance of the system for dynamic movement of the target in more indoor areas for application in robot operations.

ACKNOWLEDGMENT

This work was supported by the National Research Foundation of Korea(NRF) grant funded by the Korea government(MSIT) (No. 2022R1C1C1008306).

L. Bao is grateful for financial support of the China Scholarship Council (No. 202108260014).

REFERENCES

[1] C. Hu, S. Zhu, Y. Liang, Z. Mu, and W. Song, "Visual-Pressure Fusion for Underwater Robot Localization With Online Initialization", *IEEE Robotics and Automation Letters*, vol. 6, no. 4, pp. 8426–8433, 2021.

[2] C. Premachandra, D. N. H. Thanh, T. Kimura, and H. Kawanaka, "A study on hovering control of small aerial robot by sensing existing floor features", *IEEE/CAA Journal of Automatica Sinica*, vol. 7, no. 4, pp. 1016–1025, 2020.

[3] H. Nascimento, M. Mujica, and M. Benoussaad. "Collision avoidance in human-robot interaction using Kinect vision system combined with robot's model and data." *2020 IEEE/RSJ International Conference on Intelligent Robots and Systems (IROS)*, 2020.

[4] Y. Zhuang, Z. Syed, Y. Li, and N. El-Sheimy, Evaluation of two WiFi positioning systems based on autonomous crowdsourcing of handheld devices for indoor navigation. *IEEE Transactions on Mobile Computing*, vol. 15, no. 8, 1982-1995, 2016.

[5] N. Bai, Y. Tian, Y. Liu, Z. Yuan, Z. Xiao, and J. Zhou, A high-precision and low-cost IMU-based indoor pedestrian positioning technique. *IEEE Sensors Journal*, vol. 20, no. 12, 6716-6726, 2020.

[6] K. Bok, and J. Yoo, "RFID Based Indoor Positioning System Using Event Filtering", *Journal of Electrical Engineering and Technology*, vol. 12, no. 1, pp. 335-345, 2017.

[7] X. Zhu, J. Yi, J. Cheng, and L. He, "Adapted Error Map Based Mobile Robot UWB Indoor Positioning", *IEEE Transactions on Instrumentation and Measurement*, vol. 69, no. 9, pp. 6336–6350, 2020.

[8] S. Guo, Q. Zhao, G. Cui, S. Li, L. Kong, and X. Yang, "Behind Corner Targets Location Using Small Aperture Millimeter Wave Radar in NLOS Urban Environment", *IEEE Journal of Selected Topics in Applied Earth Observations and Remote Sensing*, vol. 13, pp. 460–470, 2020.

[9] H.W. Wehn, and P.R. Belanger, "Ultrasound-Based Robot Position Estimation", *IEEE Transactions on Robotics and Automation*, vol. 13, no. 5, pp. 682-692, 1997.

[10] F. Zafari, A. Gkelias, and K. K. Leung, "A Survey of Indoor Localization Systems and Technologies", *IEEE Communications Surveys & Tutorials*, vol. 21, no. 3, pp. 2568–2599, 2019.

[11] H. Xu, Y. Zhu, and G. Wang, "On the anti-multipath performance of UWB signals in indoor environments", *2004 4th International Conference on Microwave and Millimeter Wave Technology Proceedings*, 2004.

[12] W. Zhang, J. Liu, and J. Wang, "A multi-sensor fusion method based on EKF on granary robot", *Proceedings of the 32nd 2020 Chinese Control And Decision Conference (CCDC)*, 2020.

[13] J. Wang, M. Wang, D. Yang, F. Liu, and Z. Wen, "UWB positioning algorithm and accuracy evaluation for different indoor scenes", *International Journal of Image and Data Fusion*, vol. 12, no. 3, pp. 203–225, 2021.

[14] S. Vandermeeren and H. Steendam, "PDR/UWB Based Positioning of a Shopping Cart", *IEEE Sensors Journal*, vol. 21, no. 9, pp. 10864–10878, 2021.

[15] F. Wu, and Z. Liu, "Research on UWB / IMU Fusion Positioning Technology in Mine", *2020 International Conference on Intelligent Transportation, Big Data & Smart City (ICITBS)*, 2020.

[16] Y. Wu, W. Wang, H. Xu, and H. Kang, "Research on Indoor Sports Positioning Algorithm Based on UWB", *2021 International Conference on Control, Automation and Information Sciences (ICCAIS)*, 2021.

[17] G. Schroeer, "A Real-Time UWB Multi-Channel Indoor Positioning System for Industrial Scenarios", *2018 International Conference on Indoor Positioning and Indoor Navigation (IPIN)*, 2018.

[18] L. Ding, X. Zhu, T. Zhou, Y. Wang, Y. Jie, and Y. Su, "Research on UWB-Based Indoor Ranging Positioning Technolog and a Method to Improve Accuracy", *2018 IEEE Region Ten Symposium (Tensymp)*, 2018.

[19] Z. Li, Z. Su, and T. Yang, "Design of Intelligent Mobile Robot Positioning Algorithm Based on IMU/Odometer/Lidar", *2019 International Conference on Sensing, Diagnostics, Prognostics, and Control (SDPC)*, 2019.

[20] X. Yang, J. Wang, D. Song, B. Feng, and H. Ye, "A Novel NLOS Error Compensation Method Based IMU for UWB Indoor Positioning System", *IEEE Sensors Journal*, vol. 21, no. 9, pp. 11203–11212, 2021.

[21] Q. Fan, Y. Wu, J. Hui, L. Wu, Z. Yu, and L. Zhou, "Integrated Navigation Fusion Strategy of INS/UWB for Indoor Carrier Attitude Angle and Position Synchronous Tracking", *The Scientific World Journal*, vol. 2014, pp. 1–13, 2014.

[22] L. Yao, L. Yao, and Y.-W. Wu, "Analysis and Improvement of Indoor Positioning Accuracy for UWB Sensors", *Sensors*, vol. 21, no. 17, p. 5731, 2021.

[23] RS. Rosli, M.H. Habaebi, and M.R. Islam, "Characteristic Analysis of Received Signal Strength Indicator from ESP8266 WiFi Transceiver Module", *2018 7th International Conference on Computer and Communication Engineering (ICCCE)*, 2018.

[24] P. Pierleoni, A. Belli, L. Maurizi, L. Palma, L. Pernini, M. Paniccia, and S. Valenti, "A Wearable Fall Detector for Elderly People Based on AHRS and Barometric Sensor", *IEEE Sensors Journal*, vol. 16, no. 17, pp. 6733–6744, 2016.

[25] F. Lazzari, A. Buffi, P. Nepa, and S. Lazzari, "Numerical Investigation of an UWB Localization Technique for Unmanned Aerial Vehicles in Outdoor Scenarios", *IEEE Sensors Journal*, vol. 17, no. 9, pp. 2896–2903, 2017.

[26] J. Li, Y. Wang, Z. Chen, L. Ma, and S. Yan, "Improved Height Estimation Using Extended Kalman Filter on UWB-Barometer 3D Indoor Positioning System", *Wireless Communications and Mobile Computing*, vol. 2021, pp. 1–13, 2021.